Coulomb blockade in DNA-templated, quasi-1D nanoparticle arrays

M. S. Fairbanks,[1,*] G. J. Kearns,[2] B. C. Scannell,[1] J. E. Hutchison,[2] and R. P. Taylor[1]

[1]*Department of Physics, University of Oregon, Eugene OR 97403, USA*
[2]*Department of Chemistry, University of Oregon, Eugene OR 97403, USA*

(Dated: June 4, 2010)

We present current-voltage (I-V) measurements of quasi-1D arrays of 3.5 nm Au nanoparticles fabricated with a novel, highly parallel technique. This fabrication technique uses DNA molecules as templates for the nanoparticle arrays where the positively-charged DNA phosphate backbone interacts with the negatively-charged thiocholine ligand selected for our nanoparticles. Linear arrays are created by aligning DNA molecules across a 200 nm electrode gap via molecular combing prior to nanoparticle deposition. The I-V characteristics of these devices are consistent with Coulomb-blockaded tunnel junction arrays, though with power law exponents more commensurate with 2D sheets rather than 1D chains. We discuss the possible causes of this behavior in the context of telegraph noise-like switching in one of our devices measured at low temperatures.

PACS numbers: 73.23.Hk, 73.22.-f

Coulomb blockade (CB) occurs in systems where tunnel barriers separate a conducting island or islands from each other and the source and drain electrodes. This results in a suppression of tunneling current until an electron can pay the classical charging energy price of the conducting element, e^2/C. Since its discovery, this effect has found application in single electron transistors[1] and CB thermometers[2]. It has also been the subject of a variety of fundamental research, including theoretical and experimental treatments of blockaded arrays[3–6]. Of particular recent interest has been the self-assembly of tunneling arrays using nanometer-scale metallic particles (nanoparticles)[7–10]. In the nanoparticle arrays, the tunnel barriers are formed by the insulating shells of ligand molecules on each gold nanoparticle that prevent them from adhering to one another in solution.

The movement toward these nanoparticle-based devices is motivated in part by the potential of CB devices like single electron transistors that will operate at room temperature as a consequence of their small size (~ 1 nm) and hence large charging energies ($\geq k_B(300)$K). However, nanoparticle-based devices... (Here, a word about how the devices tend to be extended arrays and thus have electron transport properties distinct from the classical CB picture.)

In terms of a single island, an offset charge of this sort would shift the energy necessary to move a charge on to the island (eV_t). For an array of many islands, the effect of this type of disorder would be to randomize the Coulomb energy barriers of each island. An applied bias less than V_t for the array overcomes a fraction of the energy barriers in adjacent islands. Increasing the applied bias overcomes a larger fraction of barriers until eventually V_t is reached, meaning that there is at least one continuous path of off-blockade islands from source to drain. Raising the bias beyond V_t simply adds more paths until all of the islands' energy barriers are overcome, and the I-V characteristic resembles that of a single off-blockade island.

In the intermediate region between threshold and entirely off-blockade,

$$I \sim (\frac{V}{V_t} - 1)^{\zeta} \tag{1}$$

where ζ takes on the values of 5/3 and 1 for 2D and 1D arrays respectively[11]. In the 2D case, the exponent is calculated using the Kardar-Parisi-Zhang interface model[11,12], where in this case the interface is defined by how far a mobile charge can move toward the drain electrode for a given V. In the 1D case, there is only one pathway from source to drain, meaning that as soon as $V = V_t$, all islands are necessarily off-blockade, and the behavior reverts to the single island (linear response) case. In combination with the prediction that $V_t = \alpha Ne/C_g$ in the limit $C \ll C_g$, the model sets out a complete picture for the zero-temperature I-V characteristics of tunnel junction arrays[27].

Two of this model's limitations, namely the requirements that the thermal energy is much less than the charging energy and the inter-island capacitances are much less than an island's self-capacitance ($C \ll C_g$), are addressed by a recent extension[13]. The primary results of this extension are a derivation of the dominant V_t temperature trend,

$$\begin{aligned} V_t(T) &= V_t(0)[1 - p(T)/p_c] \\ &\approx V_t(0)[1 - 2bk_BTP(0)/p_c] \end{aligned} \tag{2}$$

,inclusion of nearest-neighbor, inter-island capacitive coupling, and the prediction that the power-law onset (Equation 1) will remain unchanged. Particularly relevant to our experiments are the first and last of these accomplishments. The first (analytical) expression in Equation 2 states that V_t will be suppressed from its zero temperature value ($V_t(0)$) as the ratio of $p(T)$ and the percolation threshold p_c, which are the fraction of tunnel junctions with no Coulomb barrier at temperature T, and the minimum fraction of junctions with no Coulomb barrier that guarantees a continuous path of junctions from source to drain, respectively. Starting at zero T, when

the array has a distribution of Coulomb barriers (ΔE) set by randomly distributed background charges, raising T gradually overcomes a larger and larger fraction of the Coulomb barriers until a single path connects source and drain at p_c.

Assuming a relatively flat distribution of ΔE's in the tunnel junction array, $p(T)$ can be approximated by $2bk_BTP(0)$ (Equation 2), where b depends on the density of states in an island (nanoparticle)[13] and $P(0)$ is a factor that depends primarily on the ratio of the inter-island capacitance and the total capacitance of an island.

The model was developed to extend the zero temperature model developed by Middleton[11], and was validated directly[7] and via comparison to experiments in the literature[8,14]. We will be comparing our results to this model.

In the first step in fabricating our devices, precursor Au nanoparticles with tetraoctylammonium bromide (TOAB) ligand shells were prepared as detailed in[15], resulting in a deep red solution. In order to bind to the anionic backbone of the λ-DNA template molecules, these nanoparticles must be given a cationic ligand shell. A thiocholine (N,N,N-trimethylaminoethanethiol iodide) ligand, which is known to produce close-packed nanoparticles along the DNA strand[16], was used for our devices. The TOAB ligand was replaced with the thiocholine via a biphasic ligand exchange reaction at room temperature as detailed in[17,18]. After this process, the nanoparticles were characterized via ultraviolet-visible spectroscopy and transmission electron microscopy (TEM) to confirm that the appropriate Au particle diameter was achieved. For the nanoparticles in our devices, the spectrum confirmed the presence of nanoparticles greater than 2 nm in diameter. TEM image analysis indicated a mean core diameter of 3.5 nm $\pm$1.2 nm with a ligand shell $\approx$ 0.7 nm in thickness.

In order to electrically interface with nanoscale devices like these nanoparticle arrays, there is generally a need for more 'macro-scale' contacts. Many fabrication techniques deposit the nanoscale objects on the substrate first, e.g. semiconductor nanowires or carbon nanotubes, and use electron beam lithography (EBL) to 'draw' electrodes to the nanodevices' positions. The process is reversed for our nanoparticle arrays. In addition, the ability to form our narrow nanoparticle arrays reliably is influenced by the electrode geometry.

An issue of primary importance is to achieve electrical isolation of the nanoparticle arrays. To this end, we use silicon wafers that have a thick (3 μm) thermal oxide grown on the surface. A rough calculation using SiO_2's worst-case bulk resistivity, 10^{14} Ω·m, estimates the minimum resistance path to short the device to be $\sim$ 10 TΩ. This estimate gives a reasonable expectation of effectively complete electrical isolation from the Si substrate and between the electrode pairs with no connecting nanoparticle array.

Starting with these thick oxide wafers, standard photo- and electron beam lithography are used to create electrical contacts of the geometry shown in Figure 1(a, b, and c). The contacts are a Cr/Au metal bilayer with thicknesses equal to 3 and 50 nm respectively.

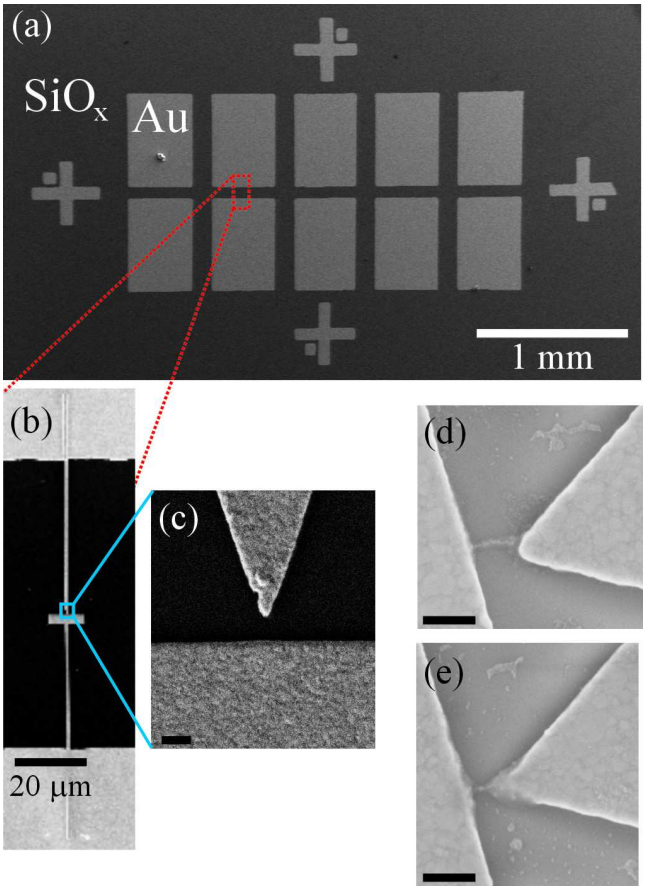

FIG. 1: Scanning electron microscope images (SEMs) of an electrode set at successively larger magnifications (a,b,c), showing the large contact pads (a), a single electron beam-defined electrode pair (b), and the electrode gap geometry (c). (d) and (e) show SEMs of the electrode gap with deposited nanoparticle arrays. Unlabeled scale bars are 250 nm (c) and 200 nm (d,e) in length.

The array of parallel pairs of electrodes enables the deposition of multiple devices in a single step, which is both useful for measurement purposes and perhaps for future applications. Aligning the DNA between the electrode pairs was done following[19]: The wafer surface is silanized to adjust the hydrophobicity (add to this section significantly) of the surface appropriately and drawn at $\approx$ 0.35 mm/s from a solution containing λ-DNA with average length = 15 μm. The DNA are aligned along the axis of the electrode pairs by the meniscus at the solution-substrate interface. The concentration of the DNA in solution is tuned with the goal that on average a single DNA strand will span each pair of electrodes, i.e. $\approx$ 1 DNA strand per 1 μm^2 area of the substrate.

After this step, the substrate is rinsed with nanopure water and floated face-down for 20 minutes in a solution containing the thiocholine-stabilized Au nanoparticles at

a concetration of 0.4 mg/mL. The nanoparticles preferentially adhere to the DNA backbone via electrostatic interactions and close-pack along its length. The face-down orientation reduces the number of nanoparticles that errantly adhere to other parts of the substrate, perhaps due to quenched charges associated with substrate crystal defects or contamination. Following nanoparticle deposition and another nanopure water rinse, the devices are complete. Based on the DNA concentration, they would ideally have a single strand, 1D character, but in practice come out in a variety of quasi-1D configurations that may consist of one to several DNA strands bundled together. This situation best explains the width of the nanoparticle arrays shown in Figure 1(d,e).

A large number of potential devices were measured on a room temperature setup, both in air and in vacuum, for testing purposes prior to the measurements described below. These tests are a simple method to determine the presence of nanoparticle arrays between a given pair of electrodes[28].

One set of completed devices was mounted on the cold finger of the ^{3}He cryostat with silver epoxy and three pairs of electrodes were contacted via ultrasonic wire bonding. Sourcing voltage, I-V curves were taken at 240 mK to establish the presence of nanoparticle arrays between each electrode pair. Two out of the three contacted devices (#2 and #3) passed detectable current. #10 passed no current, and a post-experiment SEM inspection showed that no nanoparticle array bridged the gap. To ascertain the transport characteristics of these devices, a series of I-V curves were measured as a function of temperature, 240 mK $< T \leq$ 80 K.

The measured data for the #2 and #3 devices is shown in Figure 2, (a) and (b) respectively. Their appearance, in both cases, is consistent with theory and experiment describing arrays of tunnel junctions - a blockaded region, symmetric in voltage, where no current passes through the device followed by a power law rise in current after V_t is reached. The data has a noise level that is typically $\pm$0.2 pA, though this varies from trace to trace, in one instance reaching $\pm$0.4 pA and ranging as low as $\pm$0.1 pA.

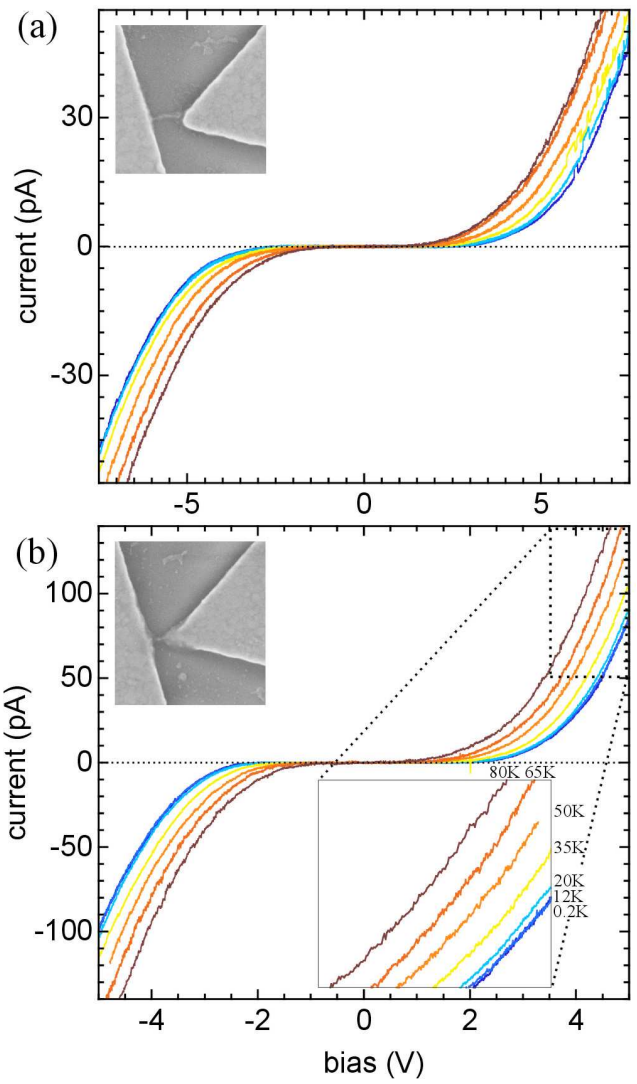

FIG. 2: Current-voltage curves for devices #2 (a) and #3 (b) are shown for temperatures ranging from $\approx$ 240 mK to 80 K. Insets show the devices corresponding to the plotted data. The zoom-in in (b) shows the correspondence between curve colors and cryostat temperature during measurement. Color-coding is identical in (a) and (b).

Two standard parameters of interest, the threshold voltage V_t and the power law exponent ζ were extracted from the I-V curves. V_t is determined systematically from inspection of the I-V data. Essentially, once the average current rises above zero and over the noise level of the data set, the threshold is said to be overcome. Another method, which involves plotting $I \times dV/dI$ vs. V and charting the V intercept[20], yields the same result within error.

This procedure was applied to both the positive and negative bias halves of the curve. According to theory, the curves should be symmetric in voltage and thus symmetric in V_t. However, the values did differ slightly (approximately $\pm$0.05 V), which was factored into the final error estimate for V_t at each temperature. The complete results of the V_t analysis are shown in Figure 3(a).

Qualitatively, the results are in agreement with the expected linear trend. Quantitatively, Equation 2 predicts a linear dependence between V_t and T. Fitting linear trends to the measured V_t values yields the dotted lines shown in Figure 3(a). If these are extrapolated up to ambient temperature, the expected temperature at which each device no longer exhibits Coulomb blockade is 125 K and 135 K for devices #2 and #3 respectively. This can be compared to a calculation of these temperatures from Equation 2. $P(0)$, the lattice geometry-dependent term, is determined from the ratio of the nanoparticle center-to-center spacing and nanoparticle radius, which = 2.8 for the average nanoparticle in our devices. This ratio

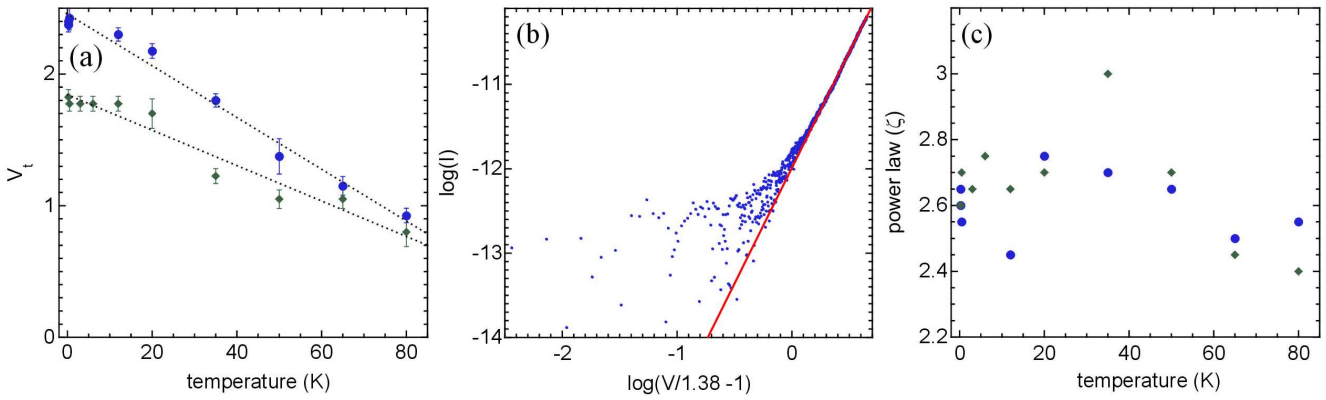

FIG. 3: (a) shows V_t vs. T for nanoparticle devices #2 and #3. Device #2 corresponds to the upper data points (blue), and device #3 is the lower data (green). Dotted lines are linear fits to each data set. (b) illustrates the procedure for determining the power law exponent (ζ) for a single data set with $V_t = 1.38$ where the red line is guide to the eye. ζ vs. T for the two devices (c) shows the spread in ζ over several measured I-Vs. The devices' data points are coded as in (a).

informs the magnitude of the inter-nanoparticle capacitances. The percolation threshold, p_c, is known for 1D chains (= 1) and large 2D networks (dependent on lattice connectivity), but for objects with intermediate geometry like our devices, it must be calculated[29]. Device #2 has $p_c = 0.80$ and device #3 has $p_c = 0.65$, which reflect their relative narrowness, ≈ 4 particles vs. ≈ 7 particles respectively. Using these simple calculations, the predicted linear slopes coming down from $V_t(0)$ are $\approx 0.002(2)$ (device #2) and 0.002(7) (device #3), which translate into blockade disappearing at $\sim$ 450 K (#2) and $\sim$ 370 K (#3).

The correspondence between the model and the observed V_t behavior is not precise, but it is important to note that these calculations are necessarily approximate. The dielectric constant of the ligand shell is not known to high accuracy, which could affect the $P(0)$ calculation somewhat. The value used here is 3 after research on a similar ligand material[9]. Also, the percolation threshold is difficult to calculate accurately, because our nanoparticle arrays appear to have an amorphous lattice geometry, variable array width, and variable individual size. This makes percolation simulations, which depend strongly on the number of nearest neighbors in the lattice, imprecise. Along these same lines, the expression for P(0) assumes identical inter-nanoparticle capacitances on a fixed lattice. The nanoparticle's diameter variation, which approaches $\sim$ 30%, will make these capacitances vary significantly. Finally, the limited extent of these quasi-1D arrays makes them more susceptible to local variations in the background charge distribution, which the model takes as uniform.

Despite these complicating issues, the linear suppression of $V_t(T)$ is retained (Figure 3(a)) in our observations, which suggests that the basis of the model is quite robust. Future calculations examining the effect of nanoparticle lattice and size perturbations ('amorphizing' the lattice) may result in better quantitative agreement with experiment for this device type.

Analysis of the power law exponent ζ is carried out as illustrated by Figure 3(b), fitting a line to a log-log plot of current vs. voltage. The voltage axis was rescaled relative to the measured V_t to match the theoretical power law form (Equation 1). In the selected example, $V_t = 1.38$ (the average of the positive and negative V_t's). Note that the fit was made to those points above zero on the x-axis. Below that, the current through the device is above threshold, but is less than approximately 2 pA. Since the noise is then comparable to the signal magnitude, the data becomes unreliable for fitting purposes.

The spread in the measured ζ's (shown vs. temperature in Figure 3(c)) is significant - approximately equal to 0.3 for both devices with a couple of exceptional cases for the #3 device. Their values are also considerably higher than those predicted by[11] (1 and 5/3 for one and two dimensions respectively). However, they are well-aligned in both instances with the power law characteristics of similar experimental systems in the literature[7,14,20,21]. All of these experiments find power laws in excess of the theoretical values for their system's dimensionality, though[14] do find a few of their carbon nanoparticle chains close to $\zeta = 1$.

The power law variance for the most directly comparable system[21], which studies strips of nanoparticles defined by EBL, is very close to what we observe. Additionally, other quasi-1D nanoparticle structures[14,22] show evidence for even greater variability. A plausible explanation for this phenomenon is the sensitivity the devices have to the local configuration of quenched background charges. The limited width of the nanoparticle arrays allows for only a few current-carrying pathways. A reconfiguration of local fixed charges changes the energy thresholds for particles in the array, thus shifting the manner in which the array responds to increasing bias. For our devices, ζ has no apparent dependence on temperature, however the spread in the the base temperature

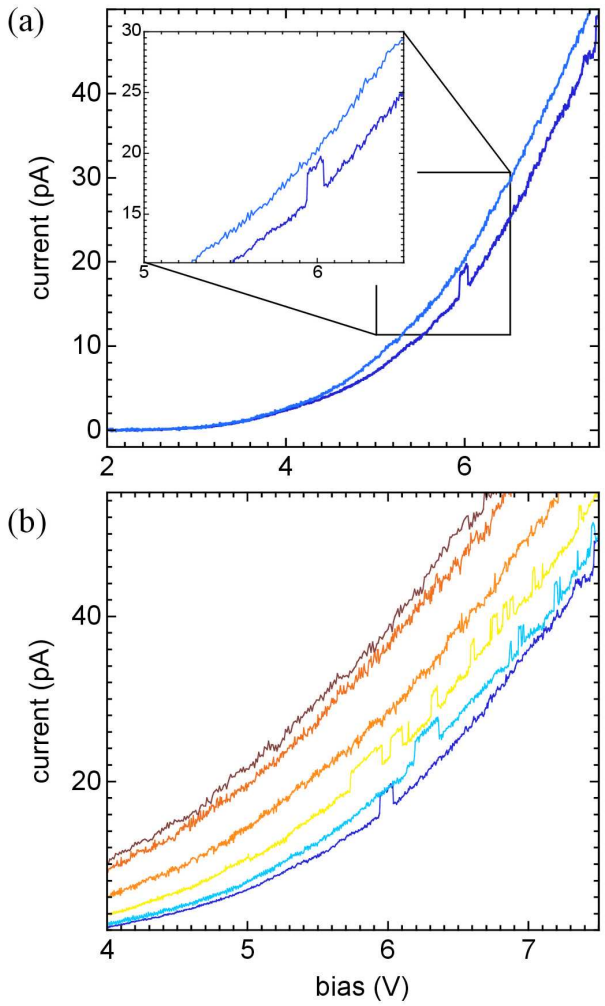

FIG. 4: 'Switching' behavior in nanoparticle device #2. A comparison of two base temperature data sets shows a single feature (a), but the switching behavior is apparent in data sets below 50 K as shown in (b).

data sets' ζ (see Figure 3(c)) suggests a temporal and/or temperature dependence for the re-configuration of background charges.

An interesting point can be observed in positive bias side of device #2's curves (Figure 4(a)). There is a small jump in the bottom curve at ≈ 6 V that takes it briefly up to the level of the top curve before reverting to its previous behavior. An instance of this occurrence is shown in Figure 4(a). This is interesting, because while the bottom curve has switched upwards, it appears to follow the top curve's power law. This switching behavior is prevalent in device #2 data sets up to and including the 35 K trace (Figure 4(b)).

The intervals of 'on' and 'off' appear random, though the jump height in current ≈ 2 pA in all cases. It is difficult to draw any strong conclusions from this limited set of observations, however we speculate that the current carrying pathway through the nanoparticle array is switching between two routes that are energetically nearly the same. The switching between them could occur due to charging/discharging of a nanoparticle or quenched substrate charging site near the pathway, which would minutely shift the energy of one path vs. the other. In this scenario, raising the temperature would eventually make the two routes effectively identical, suppressing the switching behavior. This is consistent with our observations. Similar telegraph-like switching was observed as a function of time at fixed bias in[21], also with quasi-1D chains of nanoparticles.

The experiments and analysis presented here show good correspondence with existing theoretical models and experimental results from analogous devices.

A goal for future research into these arrays may be to modify the devices such that a gate could be positioned near each one. This would be only a small change of the lithographic processes detailed earlier in the chapter, and would allow electrostatic tuning of the nanoparticles' energy spectra[30] with potentially interesting results[23,24].

The DNA/nanoparticle system could be deposited between contacts without the molecular combing step. Doing this with higher concentrations of DNA and larger electrode gaps may allow the deposition of disordered nanoparticle networks which may have a fractal geometry[31]. Because transport in tunnel junction systems is strongly dependent on their dimensionality[11], devices with a fractional dimension should exhibit behaviors distinct from one and two dimensional systems.

We acknowledge support for this project from the NSF Integrative Graduate Education and Research Traineeship (IGERT) program (G. J. Kearns and M. S. Fairbanks) and the Air Force Research Laboratory (agreement FA8650-05-1-5041). R. P. Taylor was a Cottrell Scholar of the Research Corporation.

* Electronic address: matthew.fairbanks@gmail.com

[1] M. A. Kastner, Reviews of Modern Physics **64**, 849 (1992).
[2] J. P. Pekola, K. P. Hirvi, J. P. Kauppinen, and M. A. Paalanen, Physical Review Letters **73**, 2903 (1994).
[3] R. A. Jalabert, A. D. Stone, and Y. Alhassid, Physical Review Letters **68**, 3468 (1992).
[4] J. A. Folk, S. R. Patel, S. F. Godijn, A. G. Huibers, S. M. Cronenwett, C. M. Marcus, K. Campman, and A. C. Gossard, Physical Review Letters **76**, 1699 (1996).
[5] W. G. van der Wiel, S. De Franceschi, J. M. Elzerman, T. Fujisawa, S. Tarucha, and L. P. Kouwenhoven, Reviews of Modern Physics **75**, 1 (2003).
[6] H. Grabert and M. H. Devoret, *Single Charge Tunneling: Coulomb phenomena in nanostructures*, vol. 294 of *NATO*

ASI Series (Plenum Press, 1992), 1st ed.

[7] R. Parthasarathy, X.-M. Lin, K. Elteto, T. F. Rosenbaum, and H. M. Jaeger, Physical Review Letters **92**, 076801 (2004).

[8] M. G. Ancona, W. Kruppa, R. W. Rendell, A. W. Snow, D. Park, and J. B. Boos, Physical Review B **64**, 033408 (2001).

[9] C. A. Berven, L. Clarke, J. L. Mooster, M. N. Wybourne, and J. E. Hutchison, Advanced Materials **13** (2001).

[10] T. B. Tran, I. S. Beloborodov, J. Hu, X. M. Lin, T. F. Rosenbaum, and H. M. Jaeger, Physical Review B **78**, 075437 (2008).

[11] A. A. Middleton and N. S. Wingreen, Physical Review Letters **71**, 3198 (1993).

[12] M. Kardar, G. Parisi, and Y.-C. Zhang, Physical Review Letters **56**, 889 (1986).

[13] K. Elteto, E. G. Antonyan, T. T. Nguyen, and H. M. Jaeger, Physical Review B **71**, 064206 (2005).

[14] A. Bezryadin, R. M. Westervelt, and M. Tinkham, Applied Physics Letters **74**, 2699 (1999).

[15] J. Fink, C. J. Kelly, D. Bethell, and D. J. Schiffrin, Chemistry of Materials **10**, 922 (1998).

[16] M. G. Warner and J. E. Hutchison, Nature Materials **2**, 272 (2003).

[17] G. J. Kearns, Ph.D. thesis, University of Oregon, Eugene, Oregon (2007).

[18] M. G. Warner, S. M. Reed, and J. E. Hutchison, Chemistry of Materials **12**, 3316 (2000).

[19] X. Michalet, R. Ekong, F. Fougerousse, S. Rousseaux, C. Schurra, N. Hornigold, M. van Slegtenhorst, J. Wolfe, S. Povey, J. S. Beckman, et al., Science **277**, 1518 (1997).

[20] M. G. Ancona, S. E. Kooi, W. Kruppa, A. W. Snow, E. E. Foos, L. J. Whitman, D. Park, and L. Shirey, Nano Letters **3**, 135 (2003).

[21] K. Elteto, X.-M. Lin, and H. M. Jaeger, Physical Review B **71**, 205412 (2005).

[22] L. Clarke, M. N. Wybourne, M. Yan, S. X. Cai, and J. F. W. Keana, Applied Physics Letters **71**, 617 (1997).

[23] L. S. Kuzmin, P. Delsing, T. Claeson, and K. K. Likharev, Physical Review Letters **62**, 2539 (1989).

[24] D. Davidovic and M. Tinkham, Physical Review Letters **83**, 1644 (1999).

[25] D. C. Ralph, C. T. Black, and M. Tinkham, Physical Review Letters **74**, 3241 (1995).

[26] B. Maier and J. O. Rädler, Physical Review Letters **82**, 1911 (1999).

[27] N is the number of elements in the length of the tunnel junction array, and α is a factor dependent on the array dimensionality, = 0.5 for 1D and = 0.338(1) for a 2D square lattice.

[28] Dr. Kearns also used the in-vacuum configuration of this setup to measure a series of devices at room temperature. Intriguingly, one particularly narrow device exhibited Coulomb blockade at room temperature[17]

[29] These calculations were made using a custom Mathematica routine that allowed for lattices of arbitrary length and width. A fraction of sites were turned on randomly, and the lattice was checked for percolation. This was repeated for 2000 lattice instances for a particular fraction. This was repeated for 'filling' fractions 0.0 to 1.0, charting the probability of finding a percolating path vs. fraction filled. The the middle of the transition from probability 0 to 1 determines p_c.

[30] A single nanoparticle has average energy level spacings $\approx \frac{2\pi^2\hbar^2}{m^* k_F r^3} \approx 23$ meV neglecting electron-electron interactions and using $m^* = m_0$[25]. This is well in excess of $k_B T$ at cryogenic temperatures.

[31] This is based on a fractal analysis of the AFM image in[9] of gold nanoparticle/poly-L-lysine fractured films, and research on the 2D packing statistics of DNA molecules[26]